RSC Advances

ROYAL SOCIETY OF CHEMISTRY

www.rsc.org/advances

Cite this: DOI: 10.1039/c0xx00000x

www.rsc.org/xxxxxx

High Surface Area TiO_2 Nanoparticles by a Freeze-drying Approach for Dye-sensitized Solar Cells

K. R Narendra Pai,[a] G. S. Anjusree,[a] T. G. Deepak,[a] Devika Subash,[a] Shantikumar V Nair,[a] and A. Sreekumaran Nair[a*]

Received (in XXX, XXX) Xth XXXXXXXXX 20XX, Accepted Xth XXXXXXXXX 20XX
DOI: 10.1039/b000000x

We outline a simple protocol for fabricating high surface area (~ 86 m^2/g) TiO_2 nanoparticles via. freeze-drying of a composite of a TiO_2 precursor ((Ti (IV) isopropoxide)) and a polymer (polyester) solution. The composite upon freeze-drying results in a porous mass which on subsequent sintering results in degradation of the polymer and formation of TiO_2 nanoparticles. The TiO_2 particles when employed as a photoanode of dye-sensitized solar cells shown an efficiency (η) of ~ 7%.

TiO_2 is a wide band-gap metal oxide semiconductor which is best known for its photovoltaic (dye-sensitized solar cells, DSCs), photocatalytic, self-cleaning, environmental remediation, etc. properties.[1-3] DSCs, because of the low cost of the components involved, their flexibility and environmental friendly nature, remain as one of the most promising photovoltaic technologies and continue to draw a great deal of research attention.[4] TiO_2 serves as the backbone of DSC which does the dual role of supporting the sensitizers as well as facilitating electron transport back to the transparent conducting oxide.[5-6] TiO_2 with high surface area and high porosity is essential in DSC for efficient dye adsorption and fast movement of electrolyte ions in and out of the system.[7-10]

There are several routes available for the synthesis of TiO_2 nanoparticles, the prominent being sol-gel, hydrothermal, template-assisted, electrospinning, etc.[2b,11] Commercially available TiO_2 is P-25 (from Degussa) which possess a surface area of ~ 40 m^2/g. There are high surface area TiO_2 available in the market (such as Ishihara ST01[12-13] and Hombikat UV100[14-15]) but are expensive. Electrospinning is a facile approach for making metal oxide nanofibers; however, the fibers usually have large diameter distributions (~ 100 nm to ~ 500 nm) and have low surface areas (~ 44 m^2/g) and fewer yields.[16-17] The surface areas of electrospun TiO_2 could be enhanced further through post-treatments,[18] however, this is a two-step approach and expensive. In such a scenario, we thought of devising a simple protocol by which high surface area TiO_2 could be produced for the above mentioned applications.

Thus, the present work outlines a simple protocol for getting high surface area mesoporous anatase TiO_2 for DSC applications. Titanium (IV) isopropoxide (TIP) was dissolved in a solution of polyester (which is characterized by the presence of a large number of carboxylic acid and hydroxyl groups for bonding to the TiO_2) and the polymeric solution was freeze-dried for getting a porous mass which upon sintering at high temperature results in polymer degradation and formation of TiO_2. The TiO_2 was characterized by spectroscopy, microscopy and surface area measurements. The material when used in DSC devices showed an efficiency of ~ 7% for cells of area 0.2 cm^2 with a thickness of 12 μm.

EXPERIMENTAL

Materials

Polyester (produced by the polycondensation of ethylene glycol (99.8% Min, Merck Chemicals) was produced in-house as per literature reports. Citric acid (L.R,99.5%, Nice chemicals)), titanium(IV) isopropoxide (TIP, 99.9%, Aldrich, Germany), ethanol (absolute, Fischer scientific, Leicestershire, UK), glacial acetic acid (99.9%, Fischer scientific, Leicestershire, UK), acetonitrile (99.9%, Sigma Aldrich, US), tertiary butyl alcohol (99%, Sigma Aldrich, US) and N719 dye (cisbis(4,4'-dicarboxy-2,2'-bipyridine)dithiocyanato ruthenium(II), from Solaronix, Switzerland) were used as received. Fluorine-doped tin oxide (FTO) having size 2×2 cm^2 and sheet resistance of 8-10 Ω/square was fabricated in-house using spray-pyrolysis deposition (SPD) technique.[19] The precursors of the FTO were a 0.2 M solution of dibutyltin diacetate (DBTDA) in 2-propanol and 9 M solution of ammonium fluoride (NH_4F) in water.

Preparation of the FTO plates

The glass substrate for depositing FTO was from Corning Eagle XG, USA. The DBTDA and NH_4F solutions were mixed together and sprayed onto the hot glass substrates (heated and maintained at 450 ^{0}C) for an optimum number of cycles to get a thickness of about 800 nm for the FTO coating. The FTO-coated glass were washed and dried before used for the solar cell fabrication. The sheet-resistance of the FTO was measured to be in the range of 8-10 Ω/square.

Preparation of polyester

The polymer used was synthesized as per the literature.[10,20] It is prepared by the polycondensation of an alcohol and carboxylic acid. 8.15 g of ethylene glycol was taken in a round bottom flask and heated at 80 °C in an oil bath. When temperature reached 80

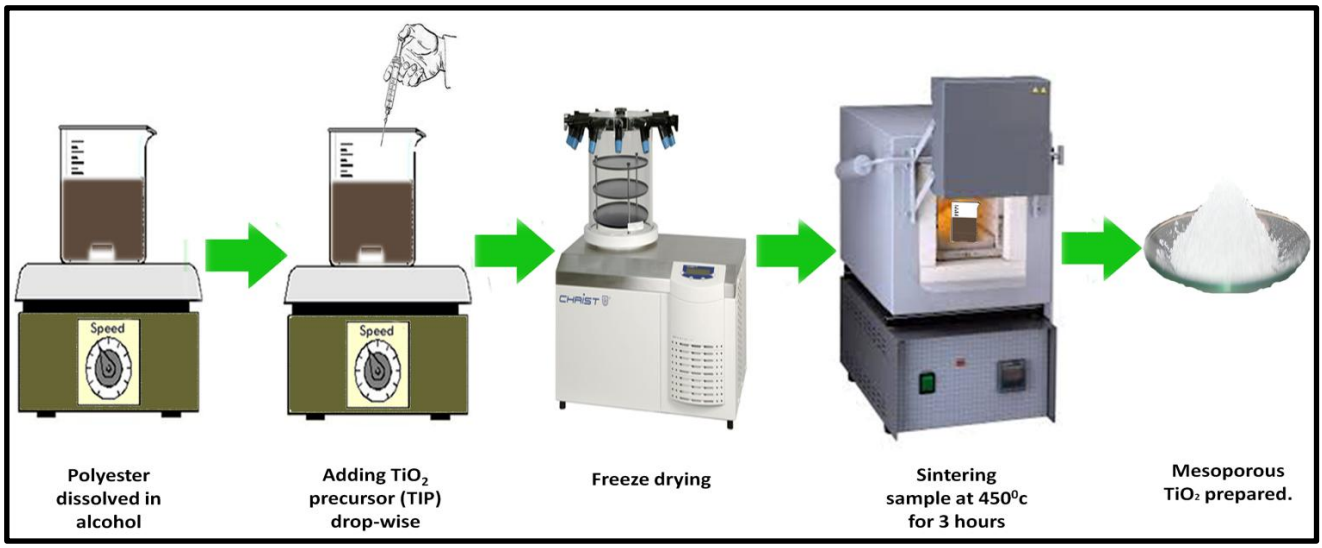

Fig. 1. A Schematic showing preparation steps for the mesoporous TiO_2.

°C, 1.42 g of TIP was added and stirred well. Once the solution becomes clear, 6.3 g of citric acid was added and temperature was increased to 100 °C. The mole ratio of ethylene glycol to citric acid was 4.5 (mass ratio of 1.3). The mixture was kept at the same temperature and stirred well for 5 h. A clear viscous solution was obtained which was then cooled down to room temperature. The average molecular weight of the polymer was estimated by an LC-Q-TOF Mass Spectrometry (Xevo G2 Q-ToF). About 20 μL of the polymer was diluted to 1 mL using LC MS grade methanol and was analyzed in positive mode by direct infusion method with a flow rate of 5 μL/min.

Preparation of mesoporous TiO_2

18.5 mL of the polyester was dissolved in 50 mL of ethanol containing 5 mL of acetic acid. To the above mixture under stirring, 2.5 mL of TIP was added. This solution was kept under stirring for another 12 h. A homogenous mixture thus obtained was subjected to freeze-drying to remove the solvent from the sample. The resulting porous mass was kept for sintering at 450 °C for 3 h to degrade the entire polymer present, which results in the formation of mesoporous TiO_2.

Characterization

Thus mesoporous TiO_2 resulted from the above method was characterized by HR-TEM (SEI Tecnai $G^2$30 operated at 300 kV) for morphology, crystallinity and structural details. Sample for HR-TEM was prepared by dispersing the sintered TiO_2 sample in methanol under sonication and then allowing a drop of this suspension to dry on a carbon-coated copper grid. X-Ray Diffractometry (XRD, wavelength =1.54Å) was employed for phase and crystal structure analysis. Poly crystalline structure and pure anatase nature of TiO_2 was confirmed with XRD. The phase purity was confirmed using X-Ray Photoelectron Spectroscopy (XPS, Kratos analytical, Ultra axis), and Raman Spectroscopy (WITEC ALPHA 300 RA) analyses. BET (Micromeritics TriStar 3000 V6.07A Instrument) was done for Surface area measurement and pore size analysis. The TiO_2 sample was dried under flowing N_2 at 350 ^{0}C overnight prior to BET measurements (under standard protocols at 77 K). DSCs were fabricated as explained below and the current-voltage (*I-V*) characteristics were measured under an illumination of 1 Sun (AM 1.5G) using a solar simulator (Newport, Oriel class A). Keithley 2400 digital source meter was used to measure the photocurrent (*I*sc) and open-circuit voltage (V_{oc}) under an applied external potential scan for an exposed area of 0.25 cm^2. IPCE spectra were measured using an Oriel Newport (tracq basic, model 77890) equipment configured for dye-sensitized solar cells.

Fabrication of photoanodes

Fabrication of photoanodes starts with coating a thin layer (~ 100 nm thick) of TiO_2 by spray pyrolysis deposition on the fluorine-doped tin oxide (FTO) glass. A paste of the mesoporous TiO_2 was prepared by mixing and mechanical grinding of the powder with a binder solution (like the polyester).

The mixture was then sonicated for 12 h which helped in forming a uniform paste of appropriate rheology required for doctor-blading. The TiO_2 paste was doctor-bladed to a suitable thicknesses (~15 µm) on $TiCl_4$ treated FTO glass plate. The fabricated photoanodes were kept in an oven at 80 °C for 30 minutes (for hardening of the mass) and then they were sintered at 450 °C for 3 h to remove the polymer. The TiO_2 film was subsequently treated with $TiCl_4$ (30 mM at 70 ^{0}C) and sintered again to 450 ^{0}C. As is well known, the $TiCl_4$ treatment produces a small rutile TiO_2 on the anatase particles in the TiO_2 film (the photoanode). When the temperature of furnace gets lowered (to 120 °C), the photoanodes were taken out and they were directly immersed in the N719 dye solution (0.5 mM in 1:1 acetonitrile-tertiary butyl alcohol mixture) for 24 h for saturate-loading of the dye. The electrodes were washed in absolute ethanol and dried in vacuum. The photoanodes were sandwiched against the platinum counter electrodes using a parafilm spacer after adding the I_3^-/I^- electrolyte on the exposed area. The cells were sealed to prevent the electrolyte leaching. The active area of the cell was 0.2 cm^2.

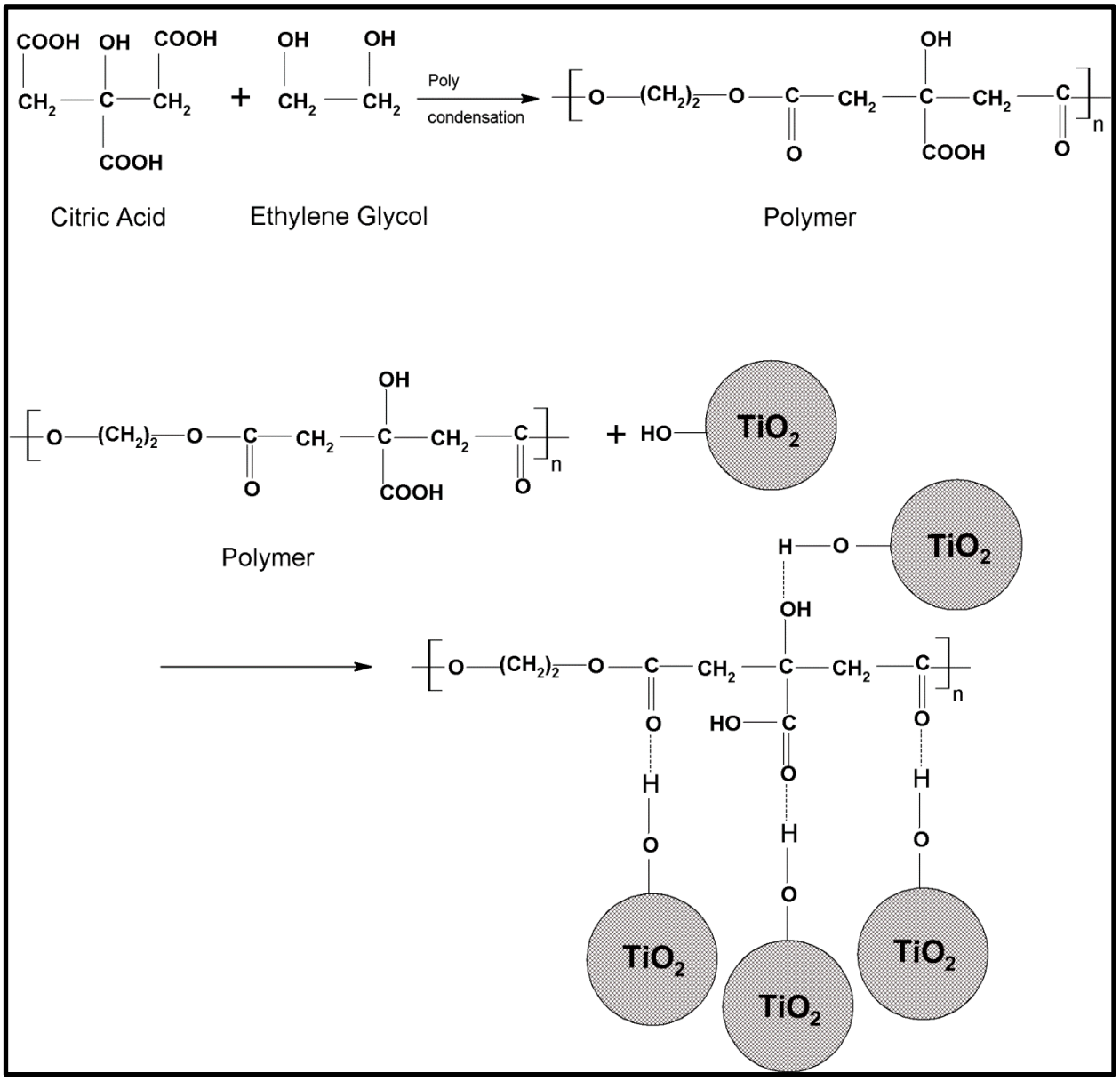

Fig.2. Schematic showing the chemical interaction between polyester and the TiO_2.

RESULTS AND DISSCUSSIONS

Polyester was prepared by the polycondensation of ethylene glycol and citric acid (Fig. 2). It is highly soluble in aqueous as well as organic solvents such as ethanol. Polyester was chosen as the surfactant for the nanoparticle preparation because of the presence of a large number of surface hydroxyl and carboxylic acid groups in the polyester backbone which facilitate hydrogen bonding with the surface hydroxyl groups of the TiO_2 thus facilitating the formation of a uniform compact mass. Fig. 1 shows an overview of the synthesis process. The amount of TiO_2 obtained from two typical syntheses is shown at the right end of the schematic showing that the process is scalable with high throughput. Considering the attributes like simplicity, time and cost-effectiveness, etc. this method offers a simple protocol for large scale synthesis of mesoporous TiO_2. The TiO_2 was characterized by TEM measurements. Large area images are shown in Fig. 3(a&b) showing agglomerated nanoparticles. An HR-TEM image is shown in Fig. 3c showing the sizes of particles and the presence of mesopores. The pores observed between the nanoparticles were in the range of 2 - 10 nm implying that the mesoporosity is due to the interparticle porosity. The average particle size was estimated to be 15 nm. A lattice-resolved image is shown in Fig. 3d showing the interplanar spacing of 0.35 nm corresponding to the prominent (101) lattice of anatase TiO_2. Inset of Fig. 3d shows a spotty SAED pattern revealing its high crystallinity. The TiO_2 was further characterized by powder XRD (Fig. 4a) and Raman (Fig. 4b) spectroscopy, respectively. Fig. 4a further confirms the pure anatase nature of the polycrystalline TiO_2. The peaks are indexed in the spectrum itself (JCPDS No. 21-1272). The sharp peak at $2\theta=25^{o}$ corresponds to the diffraction peak of anatase TiO_2 from the (101) plane.[21] The average size of the

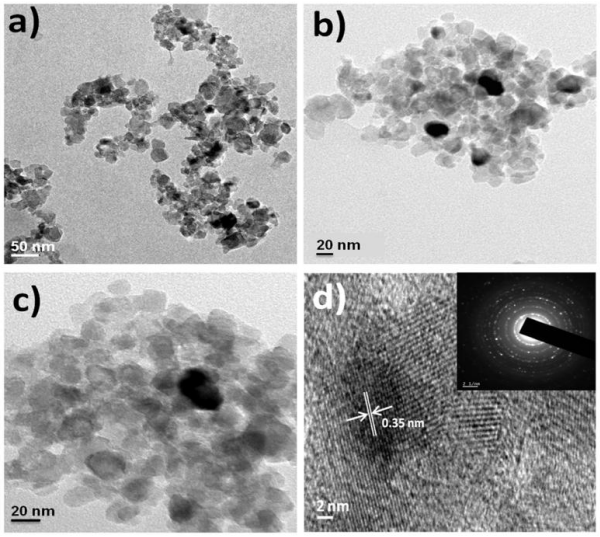

Fig. 3 a&b) TEM showing the TiO_2 nanoparticles c) HRTEM showing the interplanar spacing in TiO_2 d) SAED pattern showing the high crystallinity.

particles estimated from Scherrer equation was 12 nm which correlates well with the TEM results. The phase analysis was confirmed using Raman spectroscopy as well (Fig. 4b). According to factor group analysis, anatase has six Raman active modes (A1g + 2B1g + 3Eg). The peaks in the Raman spectrum at 166 cm^{-1}, 210 cm^{-1} and 652 cm^{-1} correspond to E_g modes and remaining two peaks at 409 cm^{-1} and 531 cm^{-1} correspond to B_{1g} and A_{1g}, respectively.[22,23] The XPS analysis was used to confirm the phase purity (Fig. 5).[2b] The binding energies of Ti 2p3/2 and Ti 2p1/2 were found at 459.39 eV and 465.02 eV, respectively, which corresponds to a spin-orbit coupling of 5.63 eV. The high-resolution spectrum of O showed 2 peaks upon de-convolution, the one at 530.1 eV corresponds to that of lattice O and that at 533 eV corresponds to the O atom from surface hydroxyl groups (chemisorbed water molecules).[24] Fig. 6 gives the nitrogen adsorption isotherm (BET) and the pore-size distribution of the TiO_2. The BET surface area was estimated to be 86 m^2/g and the pore distribution was narrow with the average pore size of about 212 Å. The average pore volume was found to be 0.46 cm^3/g. It is to be noted that since the size of the N3 dye molecules is only ~ 1 nm[2],[25] the pores in the TiO_2 electrode should be fully accessible to the dye molecules. We have found that freeze drying did improve the BET surface area of the TiO_2 as without the freeze drying process, the surface area was only 48 m^2/g for the TiO_2. This is understandable as the conventional drying process involves hard agglomeration of the composite which will create dense metal oxide particle during the cancination step. This is in contrast to the case of the freeze drying process where due to the slow evaporation of the solvent from the frozen homogenous mixture, the chemical interaction between the TiO_2 and the polyester occurs at low temperatures resulting in soft agglomerates and hence a fine TiO_2 powder of high porosity.

Low molecular weight polyester (M_n ~ 784 g/mol) was selected for the present investigation as we assumed that the ease of infiltration of TiO_2 into the short polymer chains will be high (than the polymer with longer chains) for producing a homogenous composite for freeze drying. We anticipate that the porosity (and hence the density) and the size distribution of TiO_2 could be modified by controlling the loading (infiltration) of TiO_2 on the polymer and the polymer viscosity (molecular weight). However, this needs to be investigated separately in detail in future.

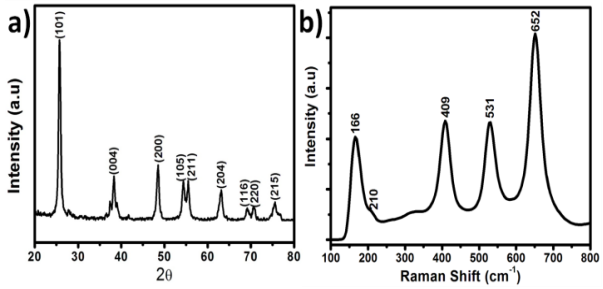

Fig. 4 a) XRD showing the pure anatase TiO_2 b) Raman spectrum of the TiO_2. The peaks are indexed in the spectra itself.

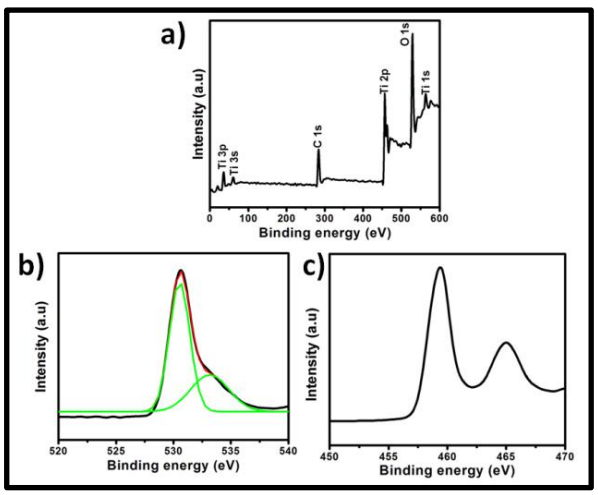

Fig. 5. XPS of TiO_2 a) wide spectra high resolution spectra of b) deconvoluted oxygen c) Ti.

DSC performance

The DSCs with different thicknesses for TiO_2 were fabricated using the procedure described in the experimental section and tested at 1 Sun under AM 1.5G conditions. The respective photovoltaic parameters are summarized in the table (Table 1). From the Table 1, it is evident that maximum performance was obtained for the DSC with a 12 µm layer thickness for TiO_2 which is in accordance with literature reports.[26] The *I-V* characteristics are shown in Fig. 7a. The DSC showed a short-circuit current density (J_{sc}) of 14.83 mA/cm^2 and an energy conversion efficiency (η) of 6.97%. In comparison, the DSC fabricated from the commercially available TiO_2 (P-25) had J_{sc} and η values of 10.37 mA/cm^2 and 5.39 %, respectively. A comparison of the *I-V* graphs of the two reveals that the major factor that contributed to the enhanced performance of the present TiO_2 was the higher J_{sc} value. To have an idea as to what was responsible for the higher J_{sc} value, we have quantified the amount of dyes in the two electrodes by dye desorption (Fig. 7c). The dye loadings in the electrodes were found to be 5.73×10^{-7} moles/cm^2 for the TiO_2 vs. 2.89×10^{-7}

Table 1. Photovoltaic parameters at different photoanode thicknesses.

Thickness (μm)	V_{oc} (V)	J_{sc} (mA/cm^2)	Fill factor (%)	Efficiency (%)
10	0.73	11.03	65.01	5.28
12	0.73	14.83	65.11	6.97
14	0.70	14.52	64.81	6.63

moles/cm^2 for the P-25. One of the reasons for the increased dye loading in the TiO_2 could be the higher surface area of the same (86 m^2/g vs. 40 m^2/g for the P-25) which increased the light harvesting capability and hence contributed to the higher J_{sc} value. This was additionally confirmed by the incident photon-to-electron conversion efficiency (IPCE) spectra of the devices (Fig. 7b). The IPCE was obtained from the relation, IPCE (%) = 1240 $J_{sc}/\lambda P_{in}$ where J_{sc} is the short-circuit current density, λ is the wavelength and P_{in} is the power of the incident light. The IPCE maximum of the TiO_2 DSC was found to be 56% compared to 45% for the P-25 and the wavelength of the IPCE maximum corresponds to the absorption maximum of the N719 dye. The main factors that contribute to the IPCE are the light harvesting efficiency, and the charge separation and collection yields.[27] As evident from dye de-loading experiments (Fig. 7c), the major parameter that has contributed to the IPCE increase was the difference in the light harvesting efficiency of the two cells, primarily determined by the difference in the dye loadings. As is well-known, in a DSC, the dye is bound to the TiO_2 surfaces through ester/cyclic ester bonds formed between the surface hydroxyl groups of the TiO_2 and the carboxylic groups of the dye.[1b,27c] Anatase TiO_2 is the preferred form over rutile for DSCs as it is rich in hydroxyl density along the (101) lattice plane.[27c] Thus, the amount of dye loaded onto the TiO_2 photoanode is a measure of both its surface area and phase purity. Since the TiO_2 film in the present case (from the freeze-dried TiO_2) is predominantly anatase and contribution from rutile phase (from the 30 mM $TiCl_4$ treatment of the film) is just negligle (see Fig. 8), the photovoltaic performance due to the enhanced dye loading could mainly be attributed to the high surface area of the TiO_2 (86 m^2/g vs. 40 m^2/g for the P-25) due to the smaller size of the particles (~ 15 nm vs. ~ 25-30 nm for the P-25) and porosity and the difference in the relative amounts of the anatase and rutile forms in the TiO_2 (~ 100% anatase in the freeze-dried TiO_2 vs. a mixture of ~ 75% anatase and ~ 25% rutile in P-25[28a]). Though there is a difference in opinion in scientific literature on the synergistic effects of anatase and rutile in the TiO_2 for photocatalysis and photovoltaics,[28-30] this needs to be investigated in the present case for DSCs through a systematic variation of the rutile and anatase phases by altering the synthetic protocol.

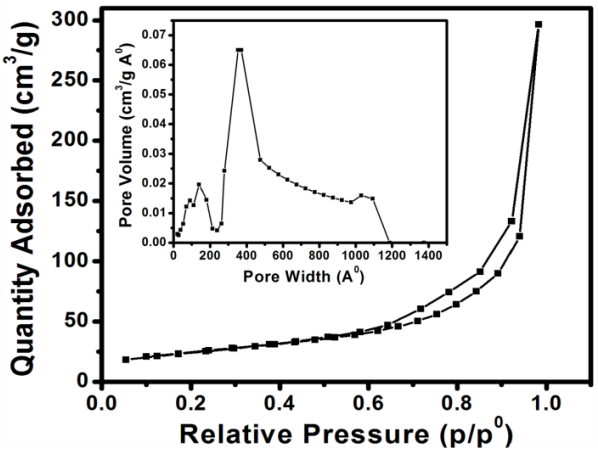

Fig. 6. BET nitrogen adsorption isotherm pattern of the TiO_2 showing the pore size distribution in the inset.

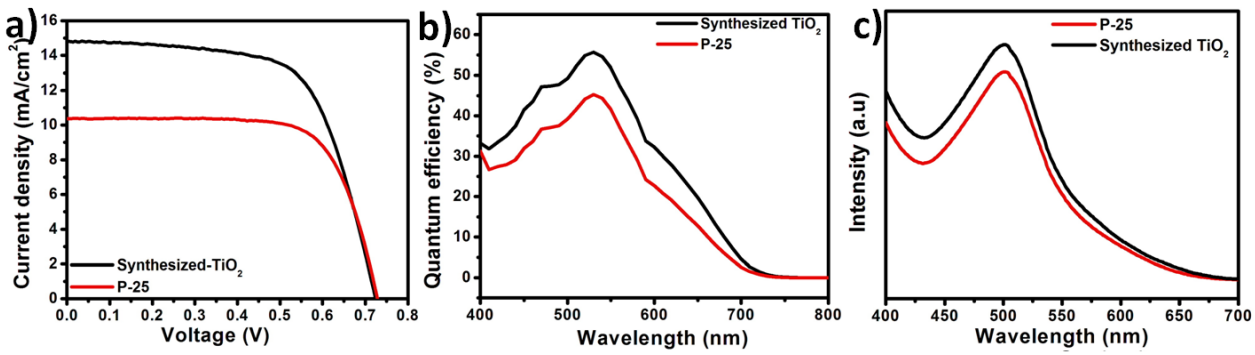

Fig.7. *I-V* characteristics of the synthesized TiO_2 compared with P-25 b) IPCE spectra, and c) dye deloading data.

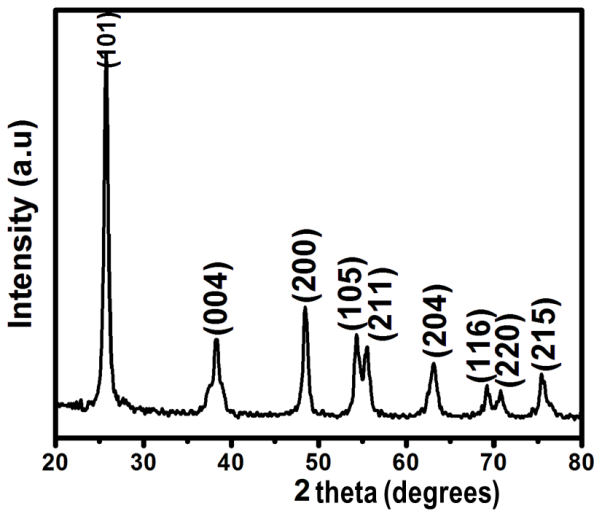

Fig. 8. XRD of the $TiCl_4$ treated TiO_2.

Conclusions

We have outlined a simple protocol for fabricating high surface area TiO_2 by freeze drying of a composite of a TiO_2 precursor and polyester, which acted as the surfactant. The porous mass obtained by the freeze drying process upon sintering resulted in TiO_2 nanoparticles of ~ 12-15 nm sizes with a high BET surface area of 86 m^2/g. The TiO_2 when employed as a photoanode of the DSC resulted in an efficiency of 7% which was higher than that of commercially available TiO_2 (5.4% for P-25). The high surface area and good phase purity of the former resulted in high dye loading and hence the better light harvesting efficiency contributed to the enhanced performance of the TiO_2 DSC device.

Acknowledgements

The authors thank Ministry of New and Renewable Energy (MNRE), Govt. of India for financial support. We also thank the reviewers whose comments have been helpful to improve the quality of the manuscript.

a Nanosolar Division, Amrita Centre for Nanosciences & Molecular Medicine, Amrita Institute of Medical Sciences, AIMS PO, Ponekkara, Kochi 682041, Kerala, India.
Email: sreekumarannair@aims.amrita.edu

References:

1. (a) B. O'Regan and M. Grätzel, *Nature*, 1991, **353**, 737–740. (b) M. Grätzel, *Acc. Chem. Res.*, 2000, **33**, 269-277.
2. (a) A. L. Linsebigler, G. Lu and J. T. Yates, *Chem. Rev.*, 1995, **95**, 735-758. (b) X. Chen and S. S. Mao, *Chem. Rev.*, 2007**, 107**, 2891-2959.
3. (a) V. A. Ganesh, S. S. Dinachali, A. S. Nair and S. Ramakrishna, *ACS Appl. Mater. Interfaces*, 2013, **5**,1527–1532. (b) M. M. Khin, A. S. Nair, V. J. Babu, R. Murugan and S. Ramakrishna, *Energy Environ. Sci.*, 2012, **5**, 8075-8109. (c) A. Fujishima, X. Zhang and D. A. Tryk, *Surf. Sci. Rep.*, 2008, 63, 515-582. (d) A. Fujishima, T. N. Rao, and D. A. Tryk, *J. Photochem. Photobiol., C*, 2000, **1**, 1-21.
4. (a) L. M. Gonçalves, V.-de. Z. Bermudez, H. A. Ribeiroa and A. M. Mendes, *Energy Environ. Sci.*, 2008, **1**, 655-667. (b) K. G. Reddy, T. G. Deepak, G. S. Anjusree, S. Thomas, S. Vadukumpully, K. R. V. Subramanian, S. V. Nair and A. S. Nair, *Phys. Chem. Chem. Phys.*, 2014, DOI: 10.1039/C3CP55448A.
5. M. Gratzel, *Accounts Chem. Res*., 2009, **42**, 1788-1798.
6. S. Zhang, X. Yang, Y. Numata and L. Han, *Energy Environ. Sci*., 2013, **6**,1443-1464.
7. Y. C. Chiang, W. Y. Cheng and S.Y. Lu, *Int. J. Electrochem. Sci.*, 2012, **7,** 6910 - 6919.
8. C. Pierre and G. M. Pajonk, *Chem. Rev.*, 2002, **102**, 4243-4265.
9. T. Y. Wei, C. H. Chen, H. C. Chien, S. Y. Lu and C. C. Hu, *Adv. Mater*., 2010, **22,** 347- 351.
10. A. S. Nair, R. Jose, Y. Shengyuan, S. Ramakrishna, *J. colloid interf sci.*, 2011, **353**, 39-45.
11. G. S. Anjusree, A. Bhupathi, A. Balakrishnan, S. Vadukumpully, K.R.V.Subramanian, N. Sivakumar, S. Ramakrishna, S. V. Nair and A.S. Nair, *RSC Adv.*, 2013, **3**, 16720-16727.
12. M. Ismail and L. Bousselmi, *Water Sci. Technol.*, 2010, **61**, 2539-48.
13. P.Wen and X.Wang, *J. Nanomaterials*, 2013, 795652.
14. A. Ramakrishnan, S. Neubert, B. Mei, L. Wang, M. Bledowski, J. Strunk, M. Muhler and R. Beranek, *Chem. Commun.*, 2012,**48**, 8556-8558.
15. A.Alonso-Tellez, R.Masson, D.Robert, N.Keller, V.Keller *J Photoch Photobio A*, 2012, **250** , 58–65.
16. A. S. Nair, Z. Peining, V. J. Babu, Y. Shengyuan and S. Ramakrishna, *Phys. Chem. Chem. Phys.*, 2011, **13**, 21248–21261.
17. Z. Ning, Y. Fub and H. Tian, *Energy Environ. Sci.*, 2010, **3**, 1170-1181.
18. (a) A. S. Nair, P. Zhu, V. J. Babu, S. Yang, T. Krishnamoorthy, R. Murugan, S. Peng, and S. Ramakrishna, *Langmuir*, 2012, **28**, 6202-6206. (b) T. A. Arun, D. K. Chacko, A. A. Madhavan, T. G. Deepak, G. S. Anjusree, T. Sara, S. Ramakrishna, S. V. Nair and A. S. Nair, *RSC Adv.*, 2014, **4**, 1421-1424. (c) D. K. Chacko, A. A. Madhavan, T. A. Arun, S. Thomas, G. S. Anjusree, T. G. Deepak, A. Balakrishnan, K. R. V. Subramanian, N. Sivakumar, S. V. Nair and A. S. Nair, *RSC Adv.*, 2013, 3, 24858-24862.
19. T. G. Deepak, G. S. Anjusree, K. R. N. Pai, D. Subash, S. V. Nair and A. S. Nair, *RSC Adv.*, 2014, **4**, 23299-23303.
20. (a) M. Pechini, US Pat., 3330697, 1967. (b) P. Zhu, A. S. Nair, S. Yang, S. Peng and S. Ramakrishna, *J. Mater. Chem.*, 2011, **21**, 12210-12212.
21. Q. Wang, S. Ito, M. Gratzel, F. Fabregat-Santiago, I. M. Sero, J. Bisquert, T. Bessho, H. Imai, *J. Phys. Chem. B*, 2006, **110**, 25210-25221.
22. C.Y. Xu, P.X. Zhang, L. Yan, *J. Raman Spectrosc.*, 2001, **32**, 862-866.
23. T. Ohsaka, F. Izumi and Y. Fujiki, *J. Raman Spectrosc.*, 1978, **7**, 321-324.
24. W. Ren, Z.Ai, *Appl. Catal. B-Environ.*, 2007, **69**, 138–144.
25. L. Du, A. Furube, K. Hara, R. Katoh and M. Tachiya, *J. Phys. Chem. C*, 2010, **114**, 8135–8143.
26. (a) S. Ito, T. N. Murakami, P. Comte, P. Liska, C. Grätzel, M. K. Nazeeruddin and M. Grätzel, *Thin Solid Films*, 2008, **516**, 4613-4619. (b) C. -Y Huanga, Y. -C Hsua, J. -G Chena, V. Suryanarayanana, K. -M Leeb, and K. -C Ho, *Sol. Energy Mater. Sol. Cells*, 2006, **90**, 2391. (d) T. G. Deepak, G. S. Anjusree, K. R. N. Pai, D. Subash, S. V Nair, and A. S. Nair, *RSC Adv.*, 2014, **4**, 23299-23303.
27. (a) Y. Chiba, A. Islam, Y. Watanabe, R. Komiya, N. Koide, and L. Han, *Jpn. J. Appl. Phys.*, 2006, **45**, L638-L640. (b) Z. Peining, A. S. Nair, Y. Shengyuan, P. Shengjie, N. K. Elumalai, and S. Ramakrishna, *J. Photochem. Photobiol., A*, 2012, **231**, 9-18. (c) M. Zuleta, T. Edvinsson, S. Yu, A. Ahmadi, G. Boschloo, M. Göthelid, and A. Hagfeldt, *Phys. Chem. Chem. Phys.* **2012**, 14, 10780-10788.
28. (a) D. C. Hurum, A. G. Agrios, K. A. Gray, T. Rajh and M. C. Thurnauer, *J. Phys. Chem. B*, 2003, 107, 4545–4549. (b) Y. K. Kho, A. Iwase, W. Y. Teoh, L. Mädler, A. Kudo and

R. Amal, *J. Phys. Chem. C*, 2010, **114**, 2821-2829. (c) B. Sun, P. G. Smirniotis, *Catal. Today*, 2003, **88**, 49-59. (d) D. O. Scanlon, C. W. Dunnill, J. Buckeridge, S. A. Shevlin, A. J. Logsdail, S. M. Woodley, C. R. A. Catlow, M. J. Powell, R. G. Palgrave, I. P. Parkin, G. W. Watson, T. W. Keal, P. Sherwood, A.Walsh and A. A. Sokol, *Nat. Mater.*, 2013, **12**, 798-801.

29. G. Li, C. P. Richter, R. L. Milot, L. Cai, C. A. Schmuttenmaer, R. H. Crabtree, G. W. Brudvig and V. S. Batista, *Dalton Trans.*, 2009, 10078–10085.

30. (a) A. Kafizas, C. J. Carmalt and I. P. Parkin, *Chem. Eur. J*, 2012, **18**, 13048-13058. (b) T. Luttrell, S. Halpegamage, J. Tao, A. Kramer, E. Sutter and M. Batzill, *Sci. Rep.*, 2014, **4**, Article number: 4043, doi:10.1038/srep04043.